

Vision-based remote 6-DOF structural displacement monitoring system using a unique marker

Haemin Jeon¹, Youngjae Kim², Donghwa Lee¹ and Hyun Myung^{*1,2}

¹*Department of Civil and Environmental Engineering, KAIST, Daejeon 305-701, Republic of Korea*

²*Robotics Program, KAIST, Daejeon 305-701, Republic of Korea*

(Received November 20, 2013, Revised March 25, 2014, Accepted April 15, 2014)

Abstract. Structural displacement is an important indicator for assessing structural safety. For structural displacement monitoring, vision-based displacement measurement systems have been widely developed; however, most systems estimate only 1 or 2-DOF translational displacement. To monitor the 6-DOF structural displacement with high accuracy, a vision-based displacement measurement system with a uniquely designed marker is proposed in this paper. The system is composed of a uniquely designed marker and a camera with a zooming capability, and relative translational and rotational displacement between the marker and the camera is estimated by finding a homography transformation. The novel marker is designed to make the system robust to measurement noise based on a sensitivity analysis of the conventional marker and it has been verified through Monte Carlo simulation results. The performance of the displacement estimation has been verified through two kinds of experimental tests; using a shaking table and a motorized stage. The results show that the system estimates the structural 6-DOF displacement, especially the translational displacement in Z-axis, with high accuracy in real time and is robust to measurement noise.

Keywords: structural health monitoring (SHM); 6-DOF displacement; vision; unique marker

1. Introduction

In the field of civil engineering, structural health monitoring (SHM) has become an important issue since civil structures are exposed to various external loads and structural deterioration is inevitable (Balageas *et al.* 2006). To measure the structural displacement, which is considered a direct indicator to assess structural safety, various sensors such as LVDTs (Linear Variable Differential Transformers), LDVs (Laser Doppler Vibrometers), GPS, and accelerometers have been used. For displacement measurement using LVDTs, a connection link between the structure and a fixed reference point is needed and only the translational displacement in one direction is measured (Park *et al.* 2013). Since it is difficult to find the reference point, this approach is not suitable for application to massive civil structures such as long-span bridges or high-rise buildings. The accuracy of LDVs or high-grade GPS such as RTK (Real-Time Kinematic)-GPS, meanwhile, is relatively high but the cost is also high (Nassif *et al.* 2005, Meng *et al.* 2004, Psimoulis and Stiros 2008). An accelerometer estimates the displacement by double integration and it has been

*Corresponding author, Professor, E-mail: hmyung@kaist.ac.kr

commonly used due to the convenience of installation and cost effectiveness (Lee *et al.* 2010, Rice *et al.* 2010). However, it is sensitive to environmental changes, such as temperature variations, and the reconstructed displacement is neither accurate nor stable due to signal drift.

Vision sensor-based displacement measurement methods are considered an attractive alternative to resolve these problems. Most vision-based displacement measurement methods install targets (markers) on the structure, and a camera located at a distance away captures images of the targets. Although they calculate the displacement directly with high accuracy, only 1 or 2-DOF translational displacement is estimated (Park *et al.* 2010, Ji and Chang 2008, Lee and Shinozuka 2006, Wahbe *et al.* 2003, Olaszek 1999, Leith *et al.* 1989, Marecos *et al.* 1969). Most vision-based displacement monitoring systems use a high quality camera and artificial targets, a structured light, or a laser range finder. In the 1960s, Marecos *et al.* proposed an infra-lamp tracking system and applied it to the Tagus River Bridge (Marecos *et al.* 1969). Laser beams have been used at the Foyle Bridge, where captured images on target screens were tracked by a fixed camera (Leith *et al.* 1989). A transputer-based feature tracking system has been studied and employed in the displacement measurement of the Humber Bridge (Stephen *et al.* 1993). Recently, high resolution cameras with optical zooming capability installed on a fixed point have been used to capture artificial landmarks using LEDs attached on the structure (Lee *et al.* 2006, Park *et al.* 2010). Another approach involved the use of a vision sensor installed on the 610 meter high Guangzhou New TV Tower in China (Ni *et al.* 2011). This system uses a high resolution camera with a telescopic lens having optical zooming capability and observes markers at a target position.

Although vision-based displacement monitoring systems can directly measure the displacement with relatively low cost, they can only measure 2-DOF translational displacement of structures. To mitigate this limitation, recent papers proposed a vision and laser-based 6-DOF displacement monitoring system (Myung *et al.* 2011, Jeon *et al.* 2011, Jeon *et al.* 2012, Jeon *et al.* 2013a, Jeon *et al.* 2013b). The system is composed of two sides facing each other, each with one or two lasers, a 2-DOF manipulator, a camera, and a screen. The lasers on each side project parallel beams to a screen on the opposite side, and a camera near the screen captures the image of the screen. By calculating the positions of the projected laser beams and rotation angles of the manipulators, the relative 6-DOF displacement between two sides can be estimated. Although the system can estimate both translational and rotational displacement, the sampling rate is relatively low (e.g., less than 5 Hz) due to the latency of communication modules (Jeon *et al.* 2013b).

To estimate 6-DOF structural displacement with high accuracy in real time, an approach using a vision sensor with a uniquely designed marker is proposed in this paper. The translational and rotational displacement between the camera and the marker can be estimated by finding a homography transformation. From a sensitivity analysis of the square-shaped conventional marker, the translational displacement in Z-axis and the rotational displacement about X and Y axes show relatively large estimation errors compared with the other components. To solve this problem, a unique marker is designed based on the sensitivity analysis. To confirm this design, Monte Carlo simulations are performed with different types of markers and different lengths of extended bars. From the simulation results, a unique marker with the extended bars was shown to reduce both translational and rotational displacement errors. Various experimental tests have been conducted to validate the performance of the proposed system. The remainder of this paper is organized as follows. The displacement estimation method using a planar marker and a camera is briefly introduced in Section 2. In Section 3, a sensitivity analysis of displacement estimation with respect to the measurement noise has been performed to design a unique marker for reducing the displacement estimation error. To validate the performance of the proposed system, various

experimental tests are conducted and the results are discussed in Section 4. In Section 5, conclusions and further research directions are discussed.

2. Vision and marker-based structural displacement measurement system

2.1 Homography-based displacement measurement system

Kinematics of the vision and marker-based displacement measurement system defines a geometric relationship between observed data, $q_i (i = 1, 2, 3 \dots)$, and displacement $p = [x, y, z, \theta, \phi, \psi]^T$ as follows (Hartley and Zisserman 2004)

$$\begin{aligned} q_i &= \begin{bmatrix} q_{i,u} & q_{i,v} & 1 \end{bmatrix}^T = \mathbf{C}[\mathbf{R}_{3 \times 3} | \mathbf{T}_{3 \times 1}] \cdot Q_i \\ &= \begin{bmatrix} f_u & 0 & o_u \\ 0 & f_v & o_v \\ 0 & 0 & 1 \end{bmatrix} \cdot \begin{bmatrix} c_\phi c_\psi & -c_\phi s_\psi & s_\phi & x \\ c_\theta s_\psi + c_\psi s_\theta s_\phi & c_\theta c_\psi - s_\psi s_\theta s_\phi & -s_\theta c_\phi & y \\ s_\theta s_\psi - c_\psi c_\theta s_\phi & s_\theta c_\psi + s_\psi c_\theta s_\phi & c_\theta c_\phi & z \end{bmatrix} \cdot \begin{bmatrix} Q_{i,x} \\ Q_{i,y} \\ Q_{i,z} \\ 1 \end{bmatrix}, \end{aligned} \quad (1)$$

where f_u , f_v , o_u , and o_v indicate the focal length and principal point in horizontal and vertical directions, and s_θ and c_θ denote $\sin\theta$ and $\cos\theta$, respectively.

As shown in Fig. 1 and Eq. (1), the relationship between the 3D points in the world frame (Q_i) and their corresponding 2D points in the pixel frame (q_i), can be represented with a homography transformation matrix composed of camera's intrinsic parameters, \mathbf{C} , and camera's extrinsic parameters, \mathbf{R} and \mathbf{T} . For simplicity, a lens distortion is not represented because the intrinsic parameters, such as focal length, principal point, and distortion parameters, are calculated in advance by using a checker board and camera calibration algorithm such as GML camera calibration toolbox (Graphics and media lab. 2013).

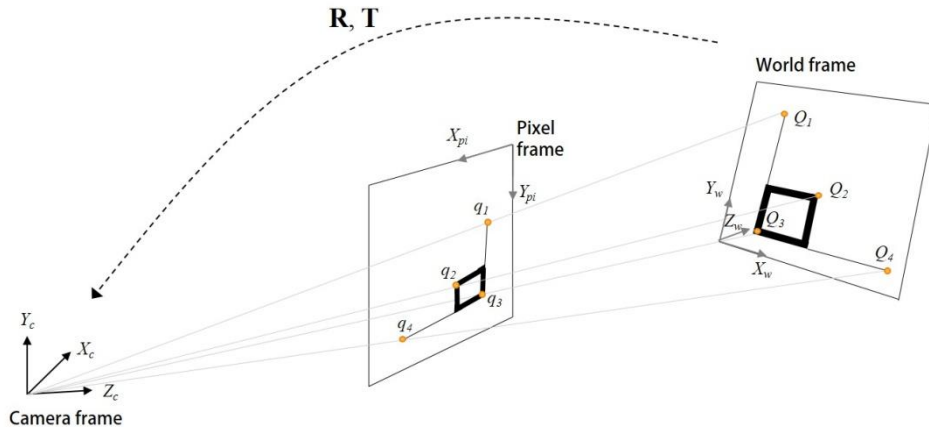


Fig. 1 Homography transformation between world and pixel frames

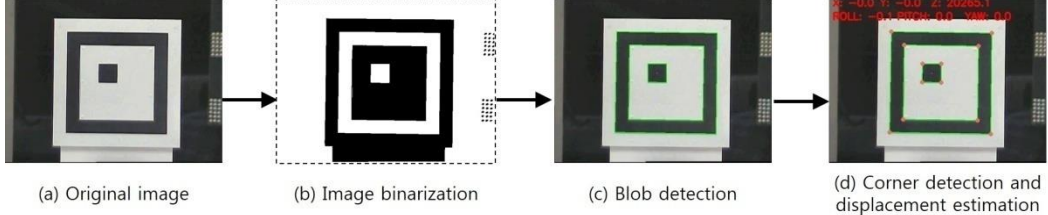


Fig. 2 Procedure of 6-DOF displacement estimation

The procedure of displacement estimation using a planar marker and a camera is shown in Fig. 2 (Lee *et al.* 2012). As shown in the figure, the camera captures the image of the marker, and then the captured image is converted to a binary image. In the binary image, the marker is detected by using a blob detection algorithm and the relative displacement between the camera and the marker is calculated by using at least four positions of detected corners of markers with a known marker's geometry. To estimate displacement, the homography transformation which transfers the world frame to pixel frame should be found. The Levenberg-Marquardt method can be used to find this homography transformation by iteratively minimizing the error of the measured and predicted positions of the corner points in the captured image. To increase the accuracy of the displacement estimation, a sub-pixel corner detection method using the orthogonal gradient of intersecting edges provided in Open CV library has been used (The Intel Co. 2013).

2.2 Sensitivity analysis of maker system

As 6-DOF displacement is estimated by minimizing the difference of the measured and estimated positions of marker's corners in the pixel frame, the accuracy of the estimation depends on the accuracy of the calculated positions on the captured image. To evaluate the sensitivity of displacement estimation according to the measurement data, the Jacobian, $\partial q_i / \partial p$, of the kinematic equation is calculated as follows

$$\begin{aligned} \frac{\partial q_i}{\partial p} &= \begin{bmatrix} \frac{\partial q_{i,u}}{\partial x} & \frac{\partial q_{i,u}}{\partial y} & \frac{\partial q_{i,u}}{\partial z} & \frac{\partial q_{i,u}}{\partial \theta} & \frac{\partial q_{i,u}}{\partial \phi} & \frac{\partial q_{i,u}}{\partial \psi} \\ \frac{\partial q_{i,v}}{\partial x} & \frac{\partial q_{i,v}}{\partial y} & \frac{\partial q_{i,v}}{\partial z} & \frac{\partial q_{i,v}}{\partial \theta} & \frac{\partial q_{i,v}}{\partial \phi} & \frac{\partial q_{i,v}}{\partial \psi} \end{bmatrix}^T \quad (2) \\ &\approx \begin{bmatrix} f_x/z' & 0 \\ 0 & f_y/z' \\ -f_x x'/z'^2 & -f_y y'/z'^2 \\ -(f_x(y-y')x'/z'^2) & -f_y((Q_{i,x}(\theta\psi-\phi)+Q_{i,y}(\theta+\phi\psi))/z'+(1-y')y'/z'^2) \\ -f_x((x-x')\psi/z'-(x-x')x'/z'^2) & f_y((x-x')\theta/z'+((x-x')y')/z'^2) \\ -f_x((Q_{i,y}+Q_{i,x}\psi)/z'+(q'x')/z'^2) & f_y((Q_{i,x}(1-\theta\phi\psi)-Q_{i,y}(\psi+\phi\theta))/z'-q'y'/z'^2) \end{bmatrix}. \end{aligned}$$

In Eq. (2), $x' = x + Q_{i,x} - Q_{i,y}\psi$, $y' = y + Q_{i,x}(\psi + \theta\phi) + Q_{i,y}(1 - \theta\phi\psi)$, $z' = z + Q_{i,x}(\theta\psi - \phi) + Q_{i,y}(\theta + \phi\psi) \approx z$, and $q' = Q_{i,x}(\theta + \phi\psi) - Q_{i,y}(\theta\psi - \phi)$ where $q_{i,u}$ and $q_{i,v}$ denote the horizontal and vertical components of q_i , and $Q_{i,x}$ and $Q_{i,y}$ denote the x and y positions of Q_i , respectively. For

simplification, the small angle approximation is used and we assume that $z \gg Q_{i,x}$ and $z \gg Q_{i,y}$ because we put the marker at a long distance away and Q_i is smaller than the marker size. As shown in the equation, both $\partial q_{i,u}/\partial z$ and $\partial q_{i,v}/\partial z$ are inversely proportional to z^2 , which makes $\partial q_i/\partial z$ relatively small in comparison with the other components such as $\partial q_i/\partial x$ and $\partial q_i/\partial y$. In other words, variation of the translational displacement in Z-axis is relatively large as the observed data change, which will be numerically verified in the Monte Carlo simulations (MCS) in the following manner:

- [1] The relative displacements, \bar{p} , between the camera and the marker are set randomly.
- [2] The positions of the corners, q , as indicated in Fig. 2(d) are calculated by using the displacement, \bar{p} , which is set in [1], and camera's intrinsic parameters.
- [3] To simulate measurement noises, an error of ± 0.2 pixels is added to the calculated q_i in [2].
- [4] From the calculated positions of marker's corners in the pixel frame, q , and known positions in the world frame, Q , the 6-DOF displacement is estimated by finding the homography transformation.

At first, 100 sets of absolute displacements, \bar{p} , are generated by adding uniform random noise of $[\pm 10, \pm 10, \pm 1000, \pm 1, \pm 1, \pm 1]$ to the initial position of $[100, -100, 10000, 5.5, 5.5, 11.5]$ (Unit: mm and deg). Then the positions of the corners, q , for each \bar{p} are calculated by using Eq. (1). After calculating q , uniform random noise of $[-0.2, 0.2]$ pixels is added to previously calculated q . Afterwards, the 6-DOF displacement is estimated by finding the homography transformation. The camera's intrinsic parameters and measurement noise level were determined from experimental tests at a distance of 10 m.

Fig. 3 shows the boxplot of the error of displacement estimation results that presents median, the upper and lower quartiles, and the largest and smallest observations of error for 100 cases. Similar with the calculated Jacobian in Eq. (2), the translational displacement in Z-axis and rotational displacement about X and Y axes show relatively large error in comparison with the other components. As the distance between the camera and the marker, z , is generally larger than the other components, e.g., 100 times larger than x and y in this simulation, the translation in Z-axis and rotational displacement about X and Y axes are more sensitive to the measurement noise.

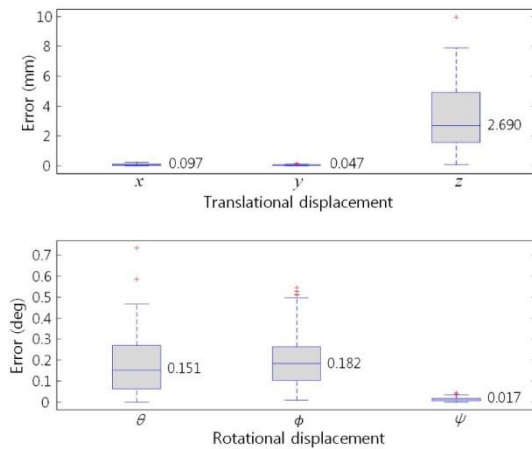


Fig. 3 Error analysis of 6-DOF displacement measurement system using a conventional planar marker

3. Design of unique marker for displacement error minimization

For design of a planner marker considering the results of the sensitivity analysis, we have performed Monte Carlo simulations with four types of planar marker with two different lengths of an extended bar. In the design of the marker, extended bars are attached with angles of 0° , 90° , and 180° to the conventional square-type marker proposed by Lee *et al.* (2012) as shown in Fig. 4. The

extended bar aligned with X-axis makes the system more sensitive to rotational displacement about Y-axis and translational displacement in Z-axis in comparison with the conventional marker (type A). In the same way, the extended bar in Y-axis makes the system more sensitive to rotational displacement about X-axis and translational displacement in Z-axis. The length of the extended bar is set to twice or four times bigger than the conventional marker size.

The procedure of MCS is identical to the simulations described in Section 2.2. The results of MCS with different designs of the planar marker and different lengths of the extended bar are shown in Table 1. The estimated displacement results of MCS are evaluated based on the normalized sum of absolute errors (NSAE_T and NSAE_R) which are defined by the following equations

$$\text{NSAE}_T = \frac{1}{3n} \sum_{i=1}^n \sum_{j=1}^3 |\bar{p}_{i,j} - p_{i,j}| \quad (3)$$

$$\text{NSAE}_R = \frac{1}{3n} \sum_{i=1}^n \sum_{j=4}^6 |\bar{p}_{i,j} - p_{i,j}| \quad (4)$$

where n is the total number of data, the subscript i indicates the i -th data and the j indicates the j -the component of the displacement in the order of x , y , z , θ , ϕ , and ψ . As shown in the table, type C marker shows the best performance regardless of the length of the extended bar. The markers of type B and D, however, show better performance only in translational displacement for both cases.

Table 1 Normalized sum of absolute errors (NSAE_T and NSAE_R) and p-values of one-way ANOVA test for four types of markers with two different lengths of the extended bar, a , when $d = 25$ cm. Compared to the conventional marker, type A, the displacement estimation using type C shows significantly reduced error for both cases

Case (a)	Marker type	NSAE_T (mm)	p-value	NSAE_R (deg)	p-value
$a = 50$ cm	Type A	1.149		0.133	
	Type B	0.590 (49% ↓)	0.0001	0.145 (9% ↑)	0.3207
	Type C	0.567 (51% ↓)	0.0001	0.068 (49% ↓)	0.0001
	Type D	0.546 (52% ↓)	0.0001	0.163 (23% ↑)	0.0263
$a = 100$ cm	Type B	1.190 (4% ↓)	0.8019	0.117 (12% ↓)	0.1710
	Type C	0.377 (67% ↓)	0.0001	0.039 (71% ↓)	0.0001
	Type D	0.396 (66% ↓)	0.0001	0.089 (33% ↓)	0.0001

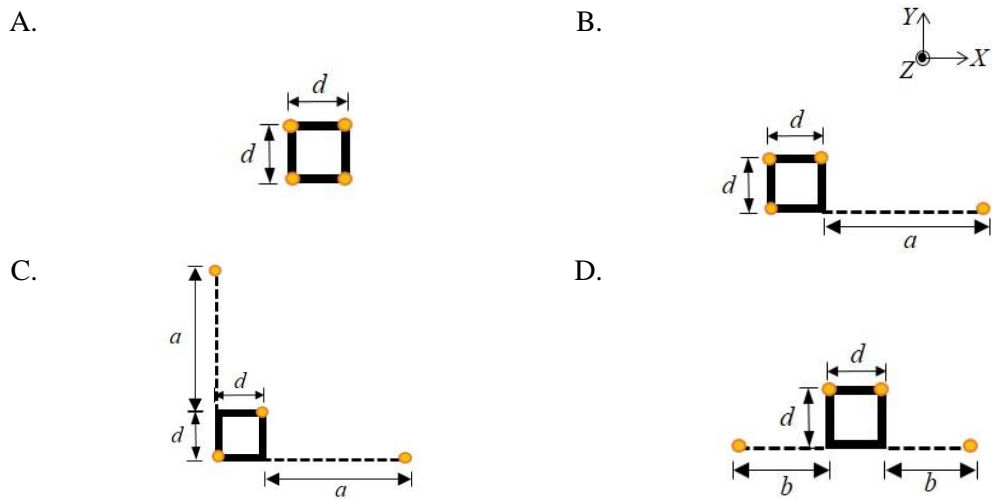
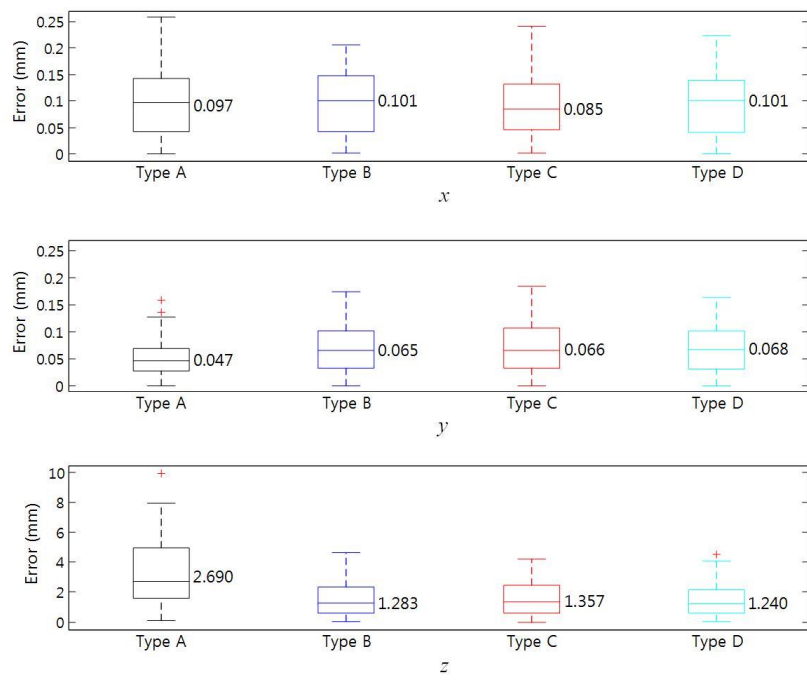


Fig. 4 Four different types of planar marker ($b = a/2$)



(a)
Continued-

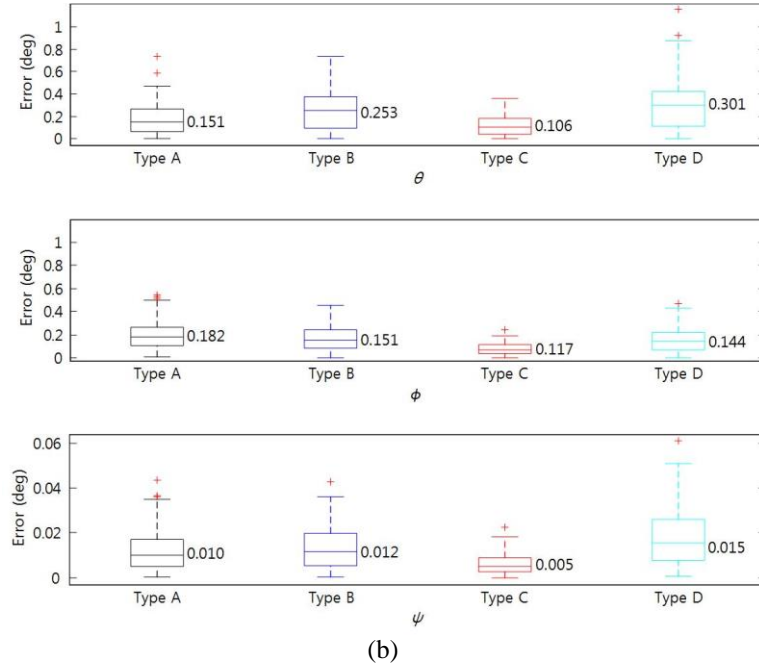


Fig. 5 Box plot of 100 Monte Carlo simulation results with four different markers ($a = 50$ cm, $d = 25$ cm). Absolute error of (a) translational and (b) rotational displacement, respectively

As shown in the table, the absolute errors of the estimated displacements using different designs of the marker are also evaluated by using a one-way ANOVA. The p-values of type C are very small for both cases, which indicates that there is a significant improvement from type A. The boxplots of the displacement estimation error with the length of extended bar of 50 cm are shown in Fig. 5. As shown in the figure, markers of type B, C, and D show better performance in translational displacement in Z-axis and rotational displacement about X and Y axes, in comparison with a conventional square-shaped planar marker, i.e., type A. As a result, type C can be selected as a novel marker design considering the results of MCS which reduces both translational and rotational displacement errors.

4. Experimental tests

To verify the performance of the proposed 6-DOF displacement estimation system using a uniquely designed planar marker, two kinds of experimental tests have been performed. The marker is laid on a shaking table or a motorized stage with a distance of 2 m and 20 m, respectively. The estimated displacements using the conventional and proposed planar markers are evaluated against the ground truth based on NSAE_T and NSAE_R . The dimensions of the planar markers used in the experimental tests are shown in Fig. 6. As shown in Fig. 6(b), the proposed marker is designed in the form of type C. In the proposed marker, smaller squares are attached at the end of the extended bars to easily detect the corners in the captured images. The digital zoom on the camera is adjusted to capture the outline of the marker as large as possible. Thus, if the marker size is enlarged, one pixel resolution becomes poor, and vice versa.

4.1 Experimental test using a shaking table

The experimental setup using a shaking table is illustrated in Fig. 7; the marker is laid on a shaking table and a camera (SCZ-2370, Samsung Techwin, Co., Ltd.) with a built-in optical zoom lens on a fixed reference point is employed. In this experiment, the shaking table is used to make artificial movement. To verify the performance of the proposed system, the estimated displacement is compared with the results from a laser displacement sensor (CD4-350, OPTEX FA Co., Ltd.) with a resolution of $40 \mu\text{m}$ (Optex-FA Co. 2007). The sampling rate of the 6-DOF displacement estimation system using planar markers and a laser displacement sensor is set to 30 Hz and 100 Hz, respectively.

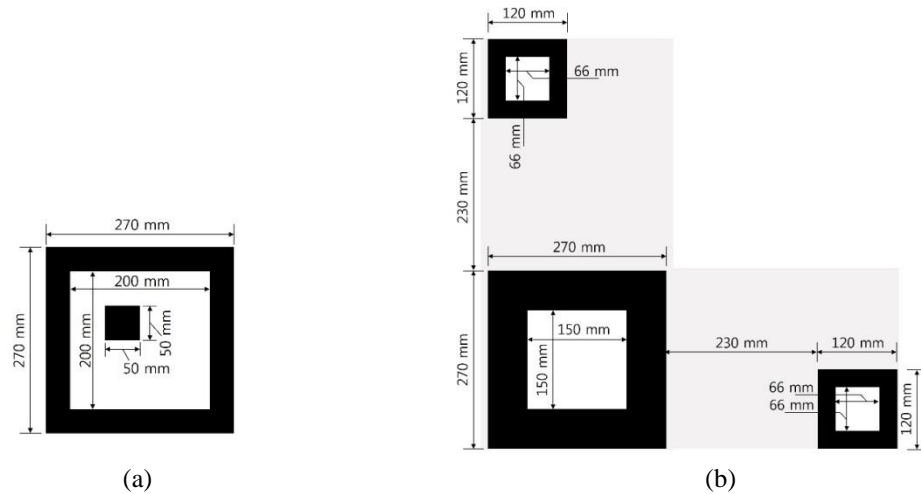


Fig. 6 Dimension of (a) the conventional planar marker proposed by Lee *et al.* (2012) and (b) the proposed planar marker

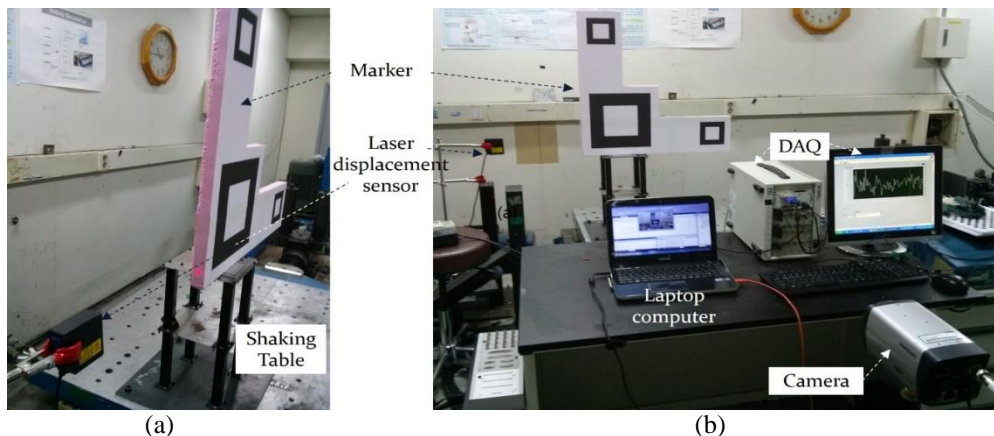
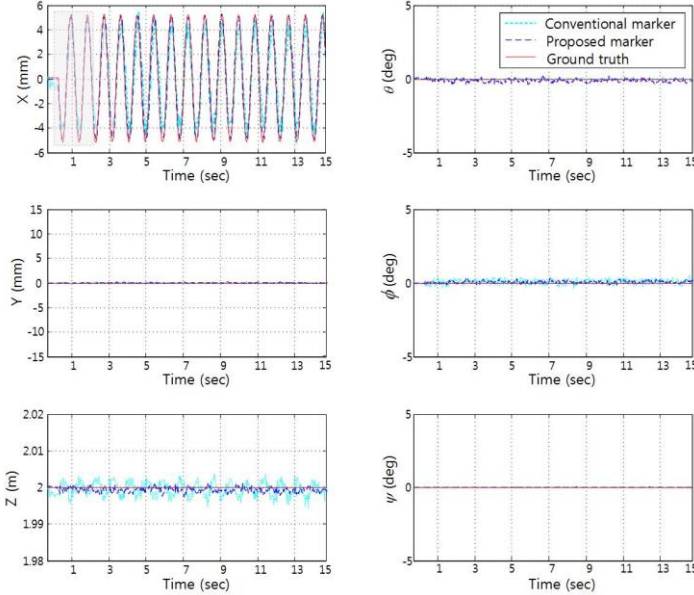


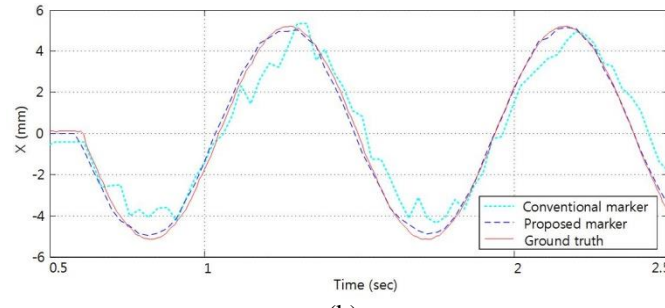
Fig. 7 Experimental setup with a shaking table. (a) Side and (b) front view of the experimental setup. The distance between the camera and the planar marker is set to 2 m

Table 2 Normalized sum of absolute errors (NSAE_T and NSAE_R) with the conventional and the proposed marker. Compared to the results from the conventional marker, the estimated displacement using the proposed marker shows significantly reduced error

Case	Marker type	NSAE _T (mm)	NSAE _R (deg)
Sinusoidal input	Conventional marker	0.8	0.1
	Proposed marker	0.3 (63% ↓)	0.1 (-)
Random input	Conventional marker	1.0	0.1
	Proposed marker	0.6 (40% ↓)	0.1 (-)



(a)



(b)

Fig. 8 Experimental results with a sinusoidal input when the distance between the camera and the marker is 2 m. (a) Estimated displacement using the conventional marker (dotted line), the proposed marker (dashed line), and laser displacement sensor (solid line). (b) Magnified plot of the estimated X-axis translational displacement for $0.5 < t < 2.5$

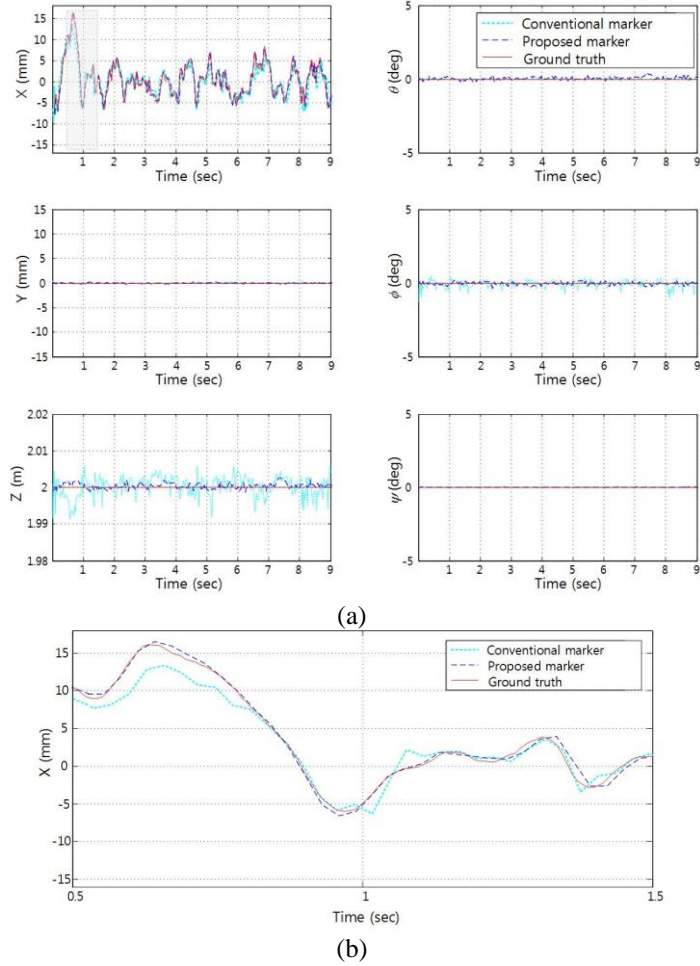


Fig. 9 Experimental results with a random input when the distance between the camera and the marker is 2 m. (a) Estimated displacement using the conventional marker (dotted line), the proposed marker (dashed line), and laser displacement sensor (solid line). (b) Magnified plot of the estimated X -axis translational displacement for $0.5 < t < 1.5$.

Two types of input voltage were applied to the shaking table. In the first case, a sinusoidal input force was set and the results are shown in Fig. 8. Fig. 8(a) shows the estimated displacements using the conventional planar marker and the proposed uniquely designed marker, and Fig. 8(b) shows a magnified plot of Fig. 8(a) between 0.5 and 2.5 sec. As shown in the figure, the estimated displacement using the proposed marker agrees with that from the laser displacement sensor and has higher accuracy in comparison with the displacement estimation using the conventional marker. In the second case, the shaking table was excited by a random force. The experimental results using two types of planar markers are shown in Fig. 9(a). A zoomed plot of Fig. 9(a) between 0.5 and 1.5 sec is shown in Fig. 9(b).

As shown in the figures, the proposed marker provides better estimation results than those

obtained using the conventional marker. In particular, the error of translational displacement in Z-axis from the designed marker is drastically reduced. NSAE_T and NSAE_R of estimated displacements using the conventional and the proposed planar markers are shown in Table 2. As shown in the table, the error of translational displacement is significantly reduced by using the proposed marker compared to the conventional marker.

4.2 Experimental test using a motorized stage

The relative 6-DOF displacement between the camera and the marker was measured by using the conventional planar marker and the proposed marker at a distance of 20 m. Artificial movement between two positions was generated by motorized stages that control translational and rotational displacement in X and about Y with a resolution of 29 nm and 5 arcmin, respectively (Thorlabs Inc. 2011). The overall experimental setup is shown in Fig. 10. Two types of markers are laid on the motorized stage as shown in Figs. 10(a) and 10(b), respectively, and the camera from a far captures the image of the marker as shown in Fig. 10(c). The sampling rate of the displacement estimation is 30 Hz, which is identical to the frame rate of the camera.

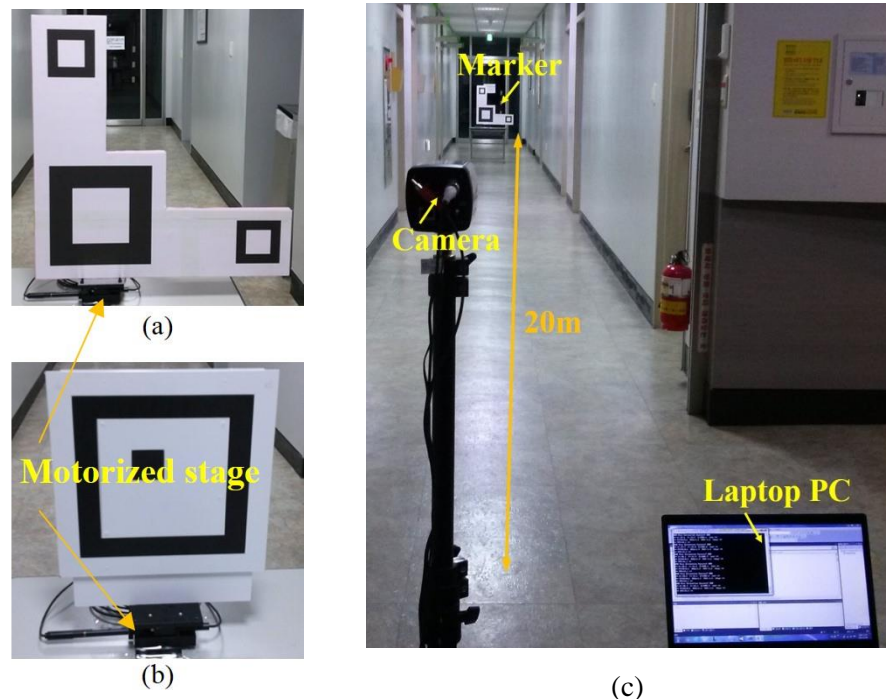


Fig. 10 Experimental setup with (a) the proposed marker and (b) the conventional marker, respectively. (c) The distance of the camera and the planar marker is set to 20 m. Movement between two positions is generated by a motorized stage installed under the planar markers

Table 3 Normalized sum of absolute errors (NSAE_T and NSAE_R) with the conventional and the proposed marker. Compared to the results from the conventional marker, the estimated displacement using the proposed marker shows significantly reduced error

Case	Marker type	NSAE_T (mm)	NSAE_R (deg)
Translation	Conventional marker	3.4	0.1
	Proposed marker	1.2 (65% ↓)	0.1 (-)
Rotation	Conventional marker	3.7	1.0
	Proposed marker	1.2 (68% ↓)	0.6 (40% ↓)

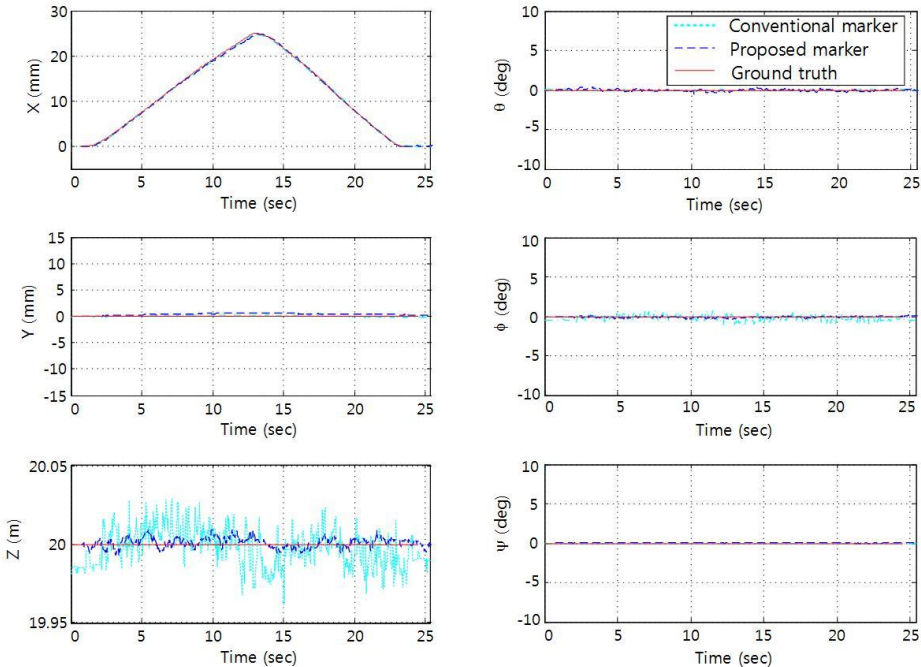


Fig. 11 Experimental results of translational displacement in X -axis. The distance between the camera and the screen was set to 20 m. Estimated displacement using the conventional marker (dotted line), the proposed marker (dashed line), and laser displacement sensor (solid line)

The experimental results of maximum translational displacement of 25 mm in X -axis and rotational displacement of 10° about Y -axis are shown in Figs. 11 and 12, respectively. As shown in the figures, the proposed marker provides higher accuracy in comparison with the conventional marker. NSAE_T and NSAE_R of estimated displacements are shown in Table 3. As shown in the table, the proposed marker estimates translational and rotational displacement with higher accuracy compared to the conventional marker. As shown in the figures and the table, the

translational and rotational displacement tracks the ground truth with relatively low error range, and in particular the errors of the translational displacement in Z-axis and rotational displacement about X and Y axes are drastically reduced as planned.

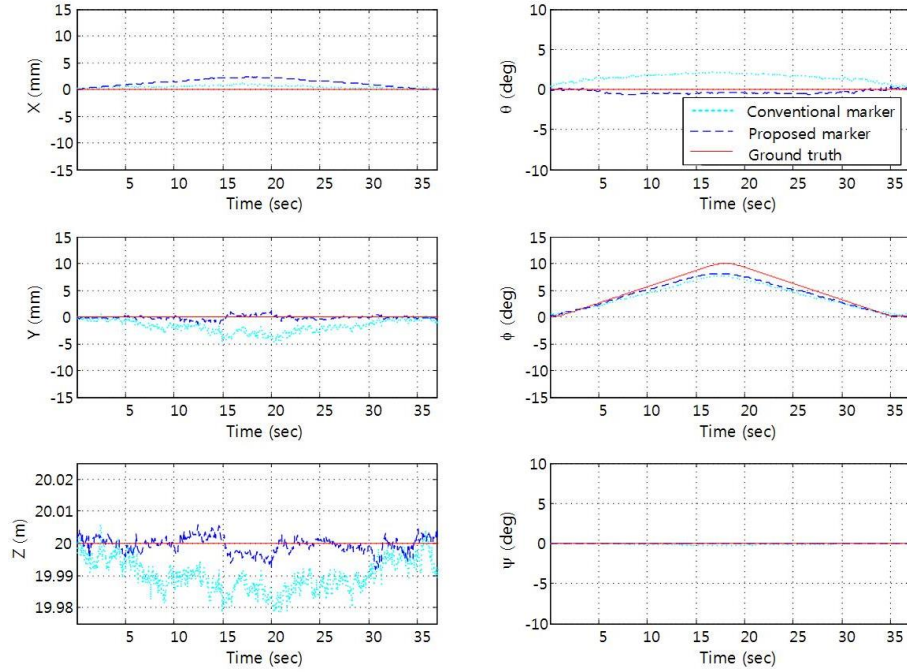


Fig. 12 Experimental results of rotational displacement about Y-axis. The distance between the camera and the screen was set to 20 m. Estimated displacement using the conventional marker (dotted line), the proposed marker (dashed line), and laser displacement sensor (solid line)

5. Conclusions

To estimate 6-DOF displacement with high accuracy, a vision and a uniquely designed marker based displacement measurement system is proposed in this paper. The sensitivity analysis using the conventional marker and Monte Carlo simulations show that the translational displacement in Z-axis and rotational displacement in X and Y axes have large errors compared with other components. To mitigate this problem, a novel marker was designed based on the sensitivity analysis. From the results of Monte Carlo simulation with four types of the planar markers and two different lengths of the extended bar, the marker with the extended bars with an angle of 90° shows the best performance in both translational and rotational displacement regardless of the length of the extended bars. The performance of the displacement estimation using the proposed marker has been verified from two kinds of experimental tests using a shaking table and a motorized stage. The results validate that the system using the proposed marker estimates 6-DOF displacement with higher accuracy in real time.

In the future, the proposed system will be applied to various civil structures to verify its applicability to real structures.

Acknowledgments

This study was supported by a grant (13SCIPA01) from Smart Civil Infrastructure Research Program funded by Ministry of Land, Infrastructure and Transport (MOLIT) of Korea government and Korea Agency for Infrastructure Technology Advancement (KAIA).

References

- Balageas, D., Fritzen, C.P. and Guemes, A. (Eds.) (2006), *Structural health monitoring*, New Jersey: John Wiley & Sons, Inc.
- Graphics and media lab. (2013), <http://graphics.cs.msu.ru/en/node/909>.
- Hartley, R.I. and Zisserman, A. (2004), *Multiple view geometry in computer vision*, Cambridge University Press.
- Jeon, H., Bang, Y. and Myung, H. (2011), "A paired visual servoing system for 6-DOF displacement measurement of structures", *Smart Mater. Struct.*, **20**(4), 045019.
- Jeon, H., Shin, J.U. and Myung, H. (2012), "Incremental displacement estimation of structures using paired structured light", *Smart Struct. Syst.*, **9**(3), 273-286.
- Jeon, H., Shin, J.U. and Myung, H. (2013a), "The displacement estimation error back-propagation (DEEP) method for a multiple structural displacement monitoring system", *Meas. Sci. Technol.*, **24**(4), 045104.
- Jeon, H., Myeong, W., Shin, J.U., Park, J.W., Jung H.J. and Myung, H. (2013b), "Experimental validation of ViSP (Visually Servoed Paired Structured Light System) for structural displacement monitoring", *IEEE/ASME Trans. Mech.*, DOI:10.1109/TMECH.2013.2290020.
- Ji, Y.F. and Chang, C.C. (2008), "Nontarget stereo vision technique for spatiotemporal response measurement of line-like structures", *J. Eng. Mech. - ASCE*, **134**(6), 466-474.
- Lee, D., Jeon, H., and Myung, H. (2012), "Vision-based 6-DOF displacement measurement of structures with a planar marker", *Proceedings of the SPIE*, San Diego.
- Lee, H.S., Hong, Y.H. and Park, H.W. (2010), "Design of an FIR filter for the displacement reconstruction using measured acceleration in low frequency dominant structures", *Int. J. Numer. Meth. Eng.*, **82**(4), 403-434.
- Lee, J.J. and Shinozuka, M. (2006), "Real-time displacement measurement of a flexible bridge using digital image processing techniques", *Exp. Mech.*, **46**(1), 105-114.
- Leith, J.G., Thompson, A. and Sloan, T.D. (1989), "A novel dynamic deflection measurement system for large structure", *Proceedings of the 4th Int. Conf. on Civil and Structural Engineering Computing*, London.
- Marecos, J., Castanheira, M. and Trigo, J. (1969), "Field observation of Tagus river suspension bridge", *J. Struct. Div. - ASCE*, **95**(4), 555-583.
- Meng, X., Roberts, G.W., Dodson, A.H., Cosser, E., Barnes, J. and Rizos, C. (2004), "Impact of GPS satellite and pseudolite geometry on structural displacement monitoring: analytical and empirical studies", *J. Geodesy*, **77**(12), 809-822.
- Myung, H., Lee, S.M. and Lee, B.J. (2011), "Paired structured light for structural health monitoring robot system", *Struct. Health Monit.*, **10**(1), 49-64.
- Nassif, H.H., Gindy, M. and Davis, J. (2005). "Comparison of laser Doppler vibrometer with contact sensors for monitoring bridge deflection and vibration", *NDT & E Int.*, **38**(3), 213-218.
- Ni, Y.Q., Wong, K.Y. and Xia, Y. (2011), "Health checks through land mark bridges to sky-high structures",

- Adv. Struct. Eng.*, **14**(1), 103-119.
- Olaszek, P. (1999), "Investigation of the dynamic characteristic of bridge structures using a computer vision method", *Measurement*, **25**(3), 227-236.
- Optex-FA (2007), *Sensor head instruction manual of displacement sensor CD4 series*, <http://www.optex-ramco.com/pdffiles/>
- Park, J.W., Lee, J.J., Jung, H.J. and Myung, H. (2010), "Vision-based displacement measurement method for high-rise building structures using partitioning approach", *NDT & E Int.*, **43**(7), 642-647.
- Park, J.W., Sim, S.H., Jung, H.J. and Spencer, B.F. (2013), "Development of a wireless displacement measurement system using acceleration responses", *Sensors*, **13**(7), 8377-8392.
- Psimoulis, P.A. and Stiros, S.C. (2008), "Experimental assessment of the accuracy of GPS and RTS for Determination of the parameters of oscillation of major structures", *Comput. Aided Civil Infrastruct. Eng.*, **23**(5), 389-403.
- Rice, J. A., Mechitov, K., Sim, S.H., Nagayama , T., Jang, S., Kim, R., Spencer, B. F., Agha, G. and Fujino , T. (2010), "Flexible smart sensor framework for autonomous structural health monitoring", *Smart Struct. Syst.*, **6**(5-6), 423-438.
- Stephen, G.A., Brownjohn, J.M.W. and Taylor, C.A. (1993), "Measurements of static and dynamic displacement from visual monitoring of the Humber bridge", *Eng. Struct.*, **15**(3), 197-208.
- The Intel Co. (2013), *The OpenCV online reference manual*, <http://docs.opencv.org>
- Thorlabs, Inc. (2011), *Thorlabs' V21 photonics catalog*, <http://www.thorlabs.com>
- Wahbeh, A.M., Caffrey, J.P. and Masri, S.F. (2003), "A vision-based approach for the direct measurement of displacements in vibrating systems", *Smart Mater. Struct.*, **12**(5), 785-794.